Ru clusters anchored on N-doped porous carbon-alumina matrix as efficient catalyst toward primary amines via reductive amination

Yushan Wu [a], Di Xu [a], Yanfei Xu [a], Xin Tian [a], Mingyue Ding [a,b,c,*]

[a] School of Power and Mechanical Engineering, Wuhan University, Wuhan 430072, China
[b] State Key Laboratory of High-efficiency Utilization of Coal and Green Chemical Engineering, Ningxia University, Yinchuan 750021, China
[c] Shenzhen Research Institute of Wuhan University, Shenzhen 518108, China

ARTICLE INFO

ABSTRACT

Efficient synthesis of primary amines via reductive amination from carbonyl compounds using NH_3 and H_2 as nitrogen and hydrogen sources is promising and challenging. Herein, we reported the ultrasmall Ru clusters bonded to the nitrogen atoms encapsulated in nitrogen-dopped carbon layers supported on alumina (Ru@NC-Al_2O_3) derived from metalated Al-MOF containing atomically dispersed Ru species, which served as highly active, selective, and reusable catalyst for the facile synthesis of primary amines. A series of carbonyl compounds including aliphatic and aryl ketones or aldehydes were converted to their corresponding primary amines under mild conditions. The excellent catalytic performance was attributed to the Ru-N coordination which could help to stabilize the Ru species and prevent their aggregation and leaching, and also ascribed to the proper Ru^0 percentage that was facilitate the hydrogenation step, as well as originated from the Lewis acid sites that was beneficial to the activation of C=N bond in intermediates.

1. Introduction

Primary amines are essential building blocks and irreplaceable intermediates in the manufacture of agrochemicals, pharmaceuticals, polyamides, and other fine chemicals [1–4]. Reductive amination of carbonyl compounds (aldehydes or ketones) to produce primary amines using NH_3 and H_2 as the nitrogen and hydrogen sources represents one of the greenest approaches with high atom efficiency, due to the sustainable resources of carbonyl compounds from renewable lignocellulosic biomass, and the waste-free process that only water as the byproduct [5–7], theoretically. Nevertheless, the synthesis of a single desired primary amine with high activity and selectivity still remains a great challenge owing to the existence of many side reactions during the process [8–11]. Here we take the furfural toward furfuryl amine as an example, which involves a quite complex reaction network. Ascribing to the presence of both ammonia and molecular hydrogen in the system, the high reactivity of aldehyde groups, as well as the instability of imine intermediate, several competitive reactions might take place. The direct hydrogenation of aldehydes to alcohol, and even excess hydrogenation of furan ring may occur. Besides, the stable intermediate Schiff base (secondary imine) could hydrogenate to the byproduct of secondary amine. Additionally, the trimerization of unstable intermediate imine to

form oligomers was also present. What's worse, the metal catalysts may be poisoned by the excess ammonia solution owing to the strong adsorption properties between the two components [12]. Thus, it is really challenging for the selective synthesis of primary amines from carbonyl compounds.

Up to now, various metal catalysts have been reported for the synthesis of primary amines from carbonyl compounds and ammonia in the atmosphere of molecular hydrogen. Among which, the low-cost and resource-rich heterogeneous metal-based catalysts such as Ni, Co and Fe catalysts are applied in the reductive amination [13–22]. Nevertheless, these catalysts usually require harsh reaction conditions, e.g., high pressure or high temperature, and their cycling stability is poor due to the sintering or leaching of active metals. Ru-based catalysts show promising potential for the reductive amination of carbonyl compounds with high selectivity [23–28]. It has been reported that the size, shape, and valance-state have important effect on the catalytic performance. Hara and co-authors found that the weak electron-donating capacity of Ru nanoparticles was beneficial to the high selectivity of primary amines [24]. In addition, the same group stated that the exposed specific (111) surface of Ru nanoparticles supported on Nb_2O_5 facilitated to the conversion of furfural to furfuryl amine [25]. Besides, Wang reported that the morphology of support had a significant effect on Ru catalyst, and

---
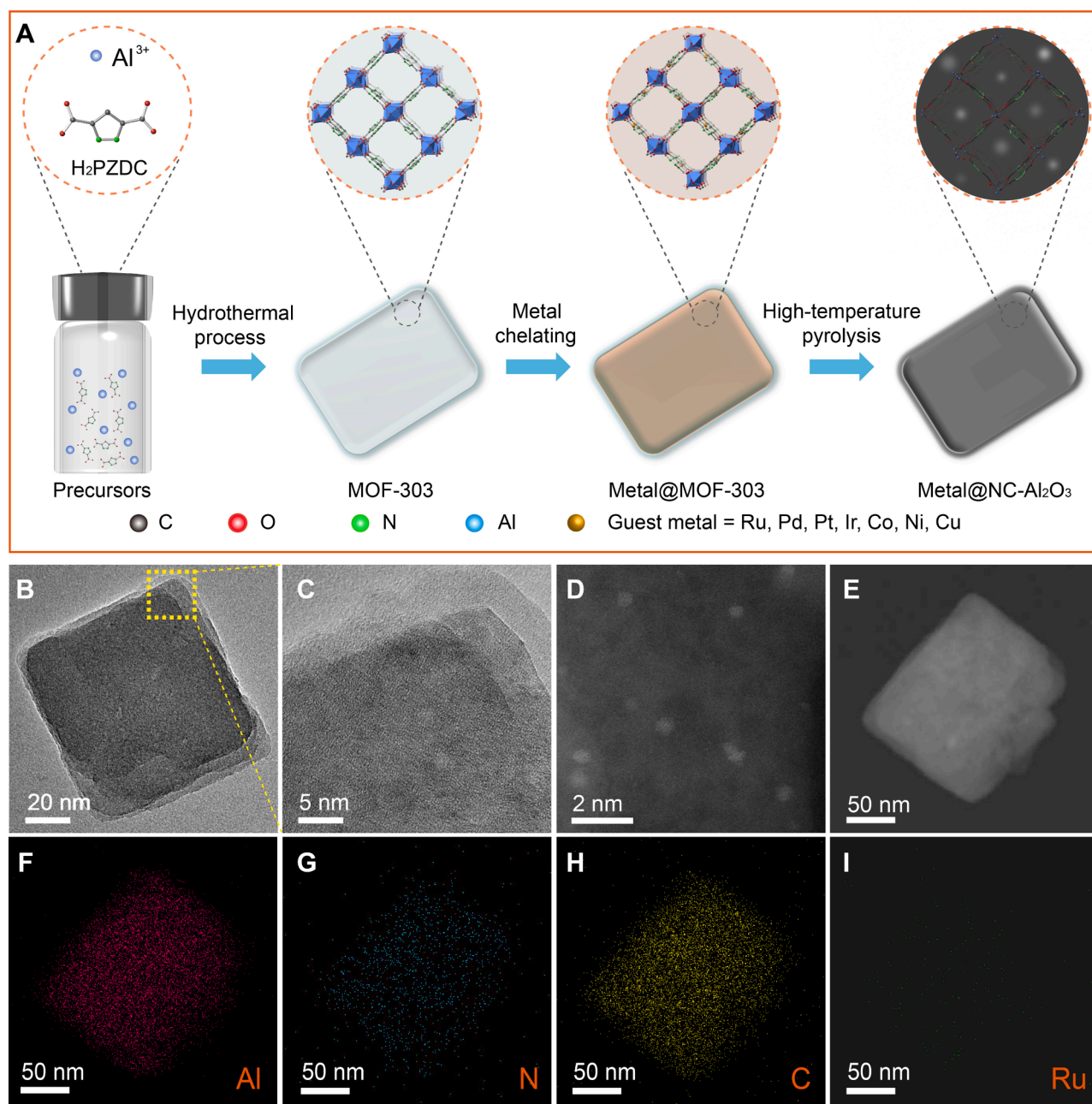
Fig. 1. . (A) Schematic illustration for the formation of xRu@NC-Al$_2$O$_3$. (B,C) HAADF-STEM images, (D) Aberration-corrected HAADF-STEM images, and (E-I) corresponding EDS element mappings of Al, C, N, and Ru for 0.5Ru@NC-Al$_2$O$_3$.

found that layered Nb$_2$O$_5$ exhibited the best performance for reductive amination due to the higher dispersion of Ru species [27]. However, the production rate of primary amine is low and the applicability of substrates is limited. Therefore, the development of metal catalysts with high stability, excellent production rate and extensive substate tolerance for the reductive amination of carbonyl compounds is highly challenging and in great demand.

Herein, we reported the ultrasmall Ru clusters encapsulated in nitrogen-dopped carbon layers supported on amorphous alumina (xRu@NC-Al$_2$O$_3$) derived from MOF chelated Ru complexes. The resulting 0.5Ru@NC-Al$_2$O$_3$ catalyst exhibited high activity and selectivity to desired primary amines, and also high stability without significant decay in the reductive amination of furfural using ammonia solution and molecular hydrogen. Further, a wide scope of carbonyl compounds (ketones/aldehydes) could be smoothly converted to their

corresponding primary amines at mild conditions, demonstrating the robust nature and universality of 0.5Ru@NC-Al$_2$O$_3$ catalyst.

2. Experimental section

2.1. Synthesis of MOF-303

MOF-303 was synthesized according to previous method [29–31]. Briefly, 3,5-pyrazoledicarboxylic acid monohydrate (22 mmol) was dispersed in 300 mL water, then NaOH (32 mmol) was added to the dispersion and sonicated until the solid was dissolved. Finally, AlCl$_3$·6 H$_2$O (22 mmol) was added to the solution with ultrasound and heated in an oil bath at 100 ℃ for 20 h. After cooling down, the white solid was collected by centrifugation and washed with water and ethanol for three times per day for three days, respectively. The obtained white powder

Table 1
Reductive amination of furfural over various catalyst.
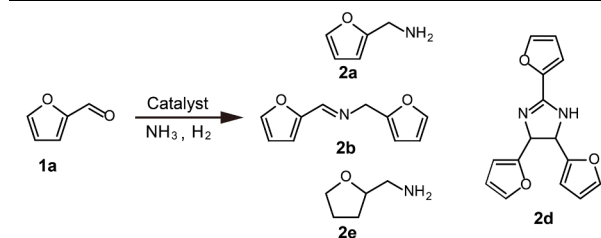
Entry	Catalyst	Yield (%)				Rate[a] (h^{-1})	CB[c]	mol%[d]
		2a	**2b**	**2d**	**2e**			
1	$1Ru@NC-Al_2O_3$	89.5	8.3	2.0	n.d.	60.3	99.8	0.49
2	$1Pt@NC-Al_2O_3$	67.1	20.8	5.2	n.d.	87.2	93.1	0.25
3	$1 Pd@NC-Al_2O_3$	39.2	43.1	1.6	n.d.	27.7	83.9	0.47
4	$1Ir@NC-Al_2O_3$	< 1	31.6	2.3	n.d.	–	34.9	0.26
5	$5Cu@NC-Al_2O_3$	< 1	12.8	8.9	n.d.	–	22.7	3.9
6	$5Co@NC-Al_2O_3$	80.3	9.2	10.2	n.d.	6.3	99.7	4.2
7	$5Ni@NC-Al_2O_3$	76.9	15.3	5.8	1.5	6.0	99.5	4.3
8	$0.2Ru@NC-Al_2O_3$	50.7	38.0	10.1	n.d.	170.6	98.8	0.1
9	$0.5Ru@NC-Al_2O_3$	96.6	2.8	< 1	n.d	132.7	99.5	0.25
10	$2Ru@NC-Al_2O_3$	78.8	4.8	< 1	14.9	26.5	98.5	0.99
11	Blank	n.d.	3.2	15.3	n.d.	–	18.5	–
12	$NC-Al_2O_3$	n.d.	5.3	20.7	n.d.	–	26.0	–

Reaction conditions: furfural (1 mmol), catalyst (50 mg), NH_3 (7 M in MeOH, 6 mL), temperature (100 ℃), H_2 pressure (2.0 MPa), reaction time (3 h), stirring speed (600 rpm). [b]n.d: not detected.
[a] Production rate = moles of product $\times$ moles of metal^{-1} $\times$ h^{-1}.
[c] CB: carbon balance.
[d] mol%: the molar ratio of metal/substrate in the catalytic system.

was dried at 150 ℃ in vacuum oven overnight to get the MOF-303.

2.2. Synthesis of M (M=Ru, Pt, Pd, Ir, Cu, Co, Ni) @MOF-303

The M@MOF-303 was synthesized by a solvothermal method, and here we take Ru@MOF-303 as an example. 500 mg activated MOF-303 was added to the acetonitrile solution containing certain amount of $RuCl_3 \cdot 3 H_2O$. The above mixture was sonicated for 5 min to obtain a uniform dispersion and subsequently heated in an oven at 80 ℃ for 24 h. The grey powder was collected by centrifugation, washed with ethanol for three times, and dried in a vacuum oven at 85 ℃ overnight. Other metal supported MOF-303 composites were prepared by the similar method which replacing the Ru salt with their corresponding metal salts.

2.3. Synthesis of M@NC-Al₂O₃

The M@NC-Al₂O₃ was synthesized by a temperature programming method. 500 mg M@MOF-303 was loaded in a porcelain boat that placed in a tube furnace. The equipment was heated from room temperature to target temperature and hold for 3 h with a rate of 5 ℃ /min under N_2 atmosphere.

2.4. Characterizations

Powder X-ray diffraction (PXRD) tests were performed on Rigaku SmartLab with filtered Cu Kα radiation (λ = 0.15405 nm) operated at 40 kV and 20 mA. N_2 adsorption-desorption isotherms were performed on Quantachrome autosorb iQ2 analyzer with ultrahigh purity N_2 in liquid nitrogen bath at 77 K. Scanning electron microscopy (SEM) images of the catalysts were obtained from a field emission SEM (Zeiss, GeminiSEM 500), and Aberration-corrected HAADF-STEM images and high-resolution transmission electron microscopy (HR-TEM) images were

collected from JEM-NEOARM (JEOL) operated at 200 kV. X-ray photoelectron spectroscopy (XPS) spectra were collected on Thermo Fisher Scientific ESCALAB250Xi using Al Kα radiation and the data were calibrated by C 1 s spectra at binding energy of 284.8 eV. Inductively coupled plasma optical emission spectroscopy (ICP-OES) was tested on Agilent ICPOES 730.

2.5. Catalytic evaluation

The catalytic performance of reductive amination was conducted in a stainless steel high-pressure reactor. Briefly, 1 mmol substrate, 50 mg catalyst, and ammonia solution (6 mL, 7 M in methanol) were added to the reactor. The autoclave was purged with H_2 (purity > 99.999%) for five times to replace the air, and charged to the desired pressure. Followed by heating at certain temperature under stirring for several hours. After the reaction finished, the steel reactor was quenched in an ice bath instantly. The liquid products were obtained by centrifugation and separation, then analyzed by using octane as the internal standard on off-line gas chromatography (GC, Fuli7980II). Conversion ($C_{conv.}$) of substrate and yield (Y_i) of products were calculated by the following equations based on carbon mole.
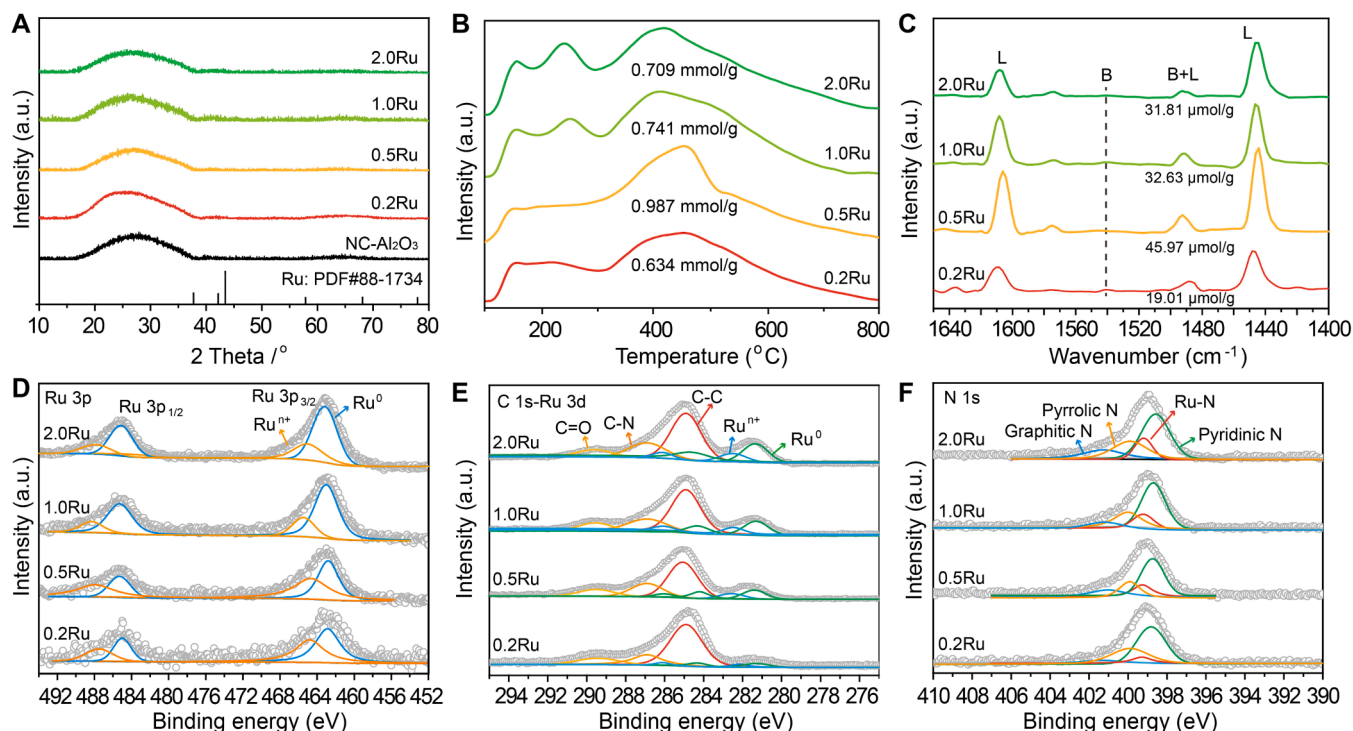
$$C_{conv}(C-mol\%) = \frac{Carbon\ moles\ in\ reactant\ reacted}{Carbon\ moles\ in\ reactant\ fed\ in} \times 100\%;$$

$$Y_i(C-mol\%) = \frac{Carbon\ moles\ in\ a\ product}{Carbon\ moles\ in\ reactant\ fed\ in} \times 100\%$$

3. Results and discussion

3.1. Structures and characterization of catalysts

Our Ru catalyst was synthesized via a simple procedure (Fig. 1A). A

Fig. 2. (A) PXRD patterns of xRu@NC-Al$_2$O$_3$ and NC-Al$_2$O$_3$. (B) NH$_3$-TPD and (C) pyridine IR for xRu@NC-Al$_2$O$_3$ complexes, the Py-IR test was operated at 200 ℃. XPS spectrum of (D) Ru 3p, (E) C 1 s-Ru 3d, and (F) N 1 s for xRu@NC-Al$_2$O$_3$ complexes.

highly porous metal-organic framework (MOF) MOF-303 with 1 D channel (Fig. S1) was employed to anchor and stabilize metal precursors. Merging activated MOF-303 with RuCl$_3$ in solvent, the Ru ions were chelated with the neighboring pair of uncoordinated N atoms from two different PZDC linkers along the MOF rods to obtain the corresponding complexes (Fig. S2). As shown in Fig. S3, these chelating processes did not change the thin square flat shape of initial polyhedrons and size distribution. The powder X-ray diffraction (PXRD) pattern of metal chelated sample Ru@MOF-303 displayed similar reflections to the pristine MOF-303 (Fig. S4), demonstrating the retention of MOF-303 crystallinity and structure. After pyrolysis at 700 ℃, the building block of MOF-303 was transformed into N-dopped porous carbon, which decorated with amorphous Al$_2$O$_3$. Meanwhile, the Ru^{3+} species coordinated with N atoms were in situ reduced to Ru clusters by the carburization of organic linkers, leading to the formation of ultrasmall Ru clusters anchored on N-dopped porous carbon-alumina complexes (xRu@NC-Al$_2$O$_3$, x denotes the loading of Ru). The actual loading of Ru species was calculated to be 0.49 wt% for 0.5Ru@NC-Al$_2$O$_3$, according to the inductively coupled plasma optical emission spectroscopy (ICP-OES, Table S1). The morphology and structures of 0.5Ru@NC-Al$_2$O$_3$ was analyzed by SEM and transmission electron microscopy (TEM). 0.5Ru@NC-Al$_2$O$_3$ could maintain the square flat shape of the original MOF-303 after high temperature treatment, while its surface became much rougher (Fig. 1B,C, and S5). The ultrasmall Ru clusters were identified by the aberration-corrected high-angle annular dark-field scanning transmission electron microscope (HAADF-STEM). Brighter and uniform spots with average diameter of 0.6 nm were observed on the N-doped porous carbon-alumina complexes (Fig. 1D), suggesting the formation of ultrasmall Ru clusters. Further, the energy dispersive spectroscopy (EDS) mappings of element Ru matched well with Al, C, and N species in a single framework, implying the uniform dispersion of Ru species across the entire architecture (Fig. 1E-1I). For control experiment, Ru catalysts (xRu@NC-Al$_2$O$_3$, x = 0.2, 1.0, 2.0) with different loading were also examined. With the increasing of Ru loading, the particle size of Ru species increased, and 1.1 nm Ru nanoparticles were detected in 2.0Ru@NC-Al$_2$O$_3$. Similarly, Al、C、N, and Ru species

were evenly distributed on the NC-Al$_2$O$_3$ support (Figs. S6-S9). Additionally, other metal catalysts (Pt, Pd, Ir, Co, Ni, and Cu) embedded in NC-Al$_2$O$_3$ were also prepared for comparison, and they were systematically characterized in detail in supporting information (Figs. S10-S18).

3.2. Catalytic performance of reductive amination over various catalysts

Here, we chose the reductive amination of furfural (**1a**) to furfuryl amine (**2a**) as the probe reaction over various catalysts due to the extensive source of furfural from biomass and the widespread application of furfuryl amine in pharmaceutical industry. Targeting the high selectivity of **2a**, different catalysts including noble metals (Ru, Pt, Pd, Ir) and none-precious metals (Cu, Co, Ni) were screened (Table 1). The conversion of **1a** was nearly 100% for all catalysts regardless of the metals used. A high yield of 89.5% **2a** was obtained over 1Ru@NC-Al$_2$O$_3$ (Table 1, entry 1), with 8.3% Schiff base (secondary imine, **2b**), and 2% 2,4,5-tris(2-furyl)imidazoline (**2d**) as the main byproducts. On the contrary, a comparably low **2a** yield of 67.1% and 39.2% was gained over Pt and Pd catalysts, whereas neither Ir nor Cu catalyst was efficient for the production of target product (Table 1, entries 2–5). In addition, transition Co and Ni metals displayed moderate **2a** yield of 80.3% and 76.9%, and trace amount of ring hydrogenated byproduct tetrahydrofurfuramine (**2e**) was formed on Ni catalyst (Table 1, entries 6 and 7). With this result in hand, we further investigated the influence of different Ru loadings on the reductive amination of **1a** for xRu@NC-Al$_2$O$_3$ (x denoted the wt% of Ru) catalyst. Obviously, only 60.7% yield of **2a** was achieved on the 0.2Ru catalyst (Table 1, entry 8), whereas it was enhanced to 96.6% over the 0.5Ru@NC-Al$_2$O$_3$ (Table 1, entry 9), corresponding to a product formation rate of 132.7 h^{-1}, ranking as one of the best performances among the heterogeneous Ru-based catalysts (Table S2). Further increasing the Ru loading, **2a** yield exhibited a decreasing trend, and large amount of **2e** byproduct was observed over 2Ru@NC-Al$_2$O$_3$ (Table 1, entry 10), ascribing to the over-hydrogenation of **2a** on furan ring. It should be noted that no target **2a** product was generated without any catalyst or in the presence of NC-Al$_2$O$_3$ (Table 1, entries 11 and 12), instead, oligomers originated from the trimerization

of imines were obtained as the byproduct, implying the indispensable role of Ru species in reductive amination. In addition, the solvent effect on reductive amination of furfural was investigated. In comparison to water, methanol was proved to be more effective in reductive amination (Table S4). These strictly control experiments, together with the comparison with more heterogeneous catalysts reported in the literatures (Table S2), unequivocally suggested the remarkable advantage of 0.5Ru@NC-Al$_2$O$_3$ catalyst with ultrasmall Ru clusters in maximizing the atom efficiency of Ru species.

3.3. Reasons for the high performance of Ru@NC-Al$_2$O$_3$ catalyst

As discussed above, the 0.5Ru@NC-Al$_2$O$_3$ catalyst displayed a superior catalytic performance compared with other catalysts, and the phase composition was first explored by PXRD analysis. The PXRD patterns for all xRu@NC-Al$_2$O$_3$ complexes displayed no obvious characteristic peaks assigning to metallic Ru or RuO$_x$, implying the homogeneous dispersion of Ru species (Fig. 2A). A broad peak in the range of 20–30° was detected, which was attributed to the (002) plane of the graphitic carbon [32,33] derived from the organic linkers of MOF. In addition, no peaks ascribing to Al$_2$O$_3$ were observed, indicating the amorphous state. The xRu@NC-Al$_2$O$_3$ complexes exhibited high Brunauer-Emmett-Teller (BET) surface areas in the range of 105–152 m^2 g^{-1}, and displayed a decreasing tendency with the increase of Ru loading (Fig. S19a). All the curves showed type IV isotherms, suggesting their mesoporous feature with average pore diameter of 10–20 nm (Fig. S19b). The high specific surface area and large pore diameter of 0.5Ru@Al$_2$O$_3$ facilitated the diffusion of reactants and desorption of target product, thus contributing to the formation of **2a**. As for 2Ru@Al$_2$O$_3$, the decreased specific surface area and pore width might lead to the low yield of **2a**, and the excessive Ru species might explain the formation of over-hydrogenated byproduct **2e**.

As shown in Fig. 2B, NH$_3$-TPD profiles revealed three main desorption peaks centered at 150 ℃, 250 ℃, and 350–500 ℃, corresponding to the weak acid, medium-strong acid, and strong acid [34–36], respectively. It was observed that both the weak and strong acid amount increased first and then decreased with the increasing of Ru loading, and 0.5Ru@NC-Al$_2$O$_3$ exhibited the highest total acid amount among the Ru catalysts (Table S5). In addition, the strong acid peaks in 0.5Ru@N-C-Al$_2$O$_3$ shifted to higher temperature in comparison to other samples, implying that the corresponding acid sites were effectively strengthened. The higher acidity was suitable for the binding of NH$_3$ molecular, and was in favor of the activation of C═N bonds in the intermediates of imines and Schiff bases via the interaction of acid sites and N atoms [5, 37,38], thus contributing to the excellent catalytic performance.

In order to further analyze the acid sites distribution of Ru catalysts, the Py-IR spectra was conducted (Fig. 2C), and the introduction of Ru species played a significant role in adjusting the acid amount of xRu@NC-Al$_2$O$_3$ catalysts. The characteristic absorption of pyridine at 1610 and 1445 cm^{-1} were observed, originated from the Lewis (L) acid sites [39,40]. While the absorbance located around 1490 cm^{-1} resulted from the B or/and L acid sites [39,40]. A band assigning to α-pyridone species, representing the presence of basic surface OH groups and acid-base pair sites, also appeared at about 1575 cm^{-1} [41]. Additionally, the extremely weak bands at 1640 and 1540 cm^{-1} suggested that very low Brønsted (B) acids sites were present on the surface of catalysts [39,40]. The pure NC-Al$_2$O$_3$ displayed a Lewis acid amount of 35.1 μmol/g (Fig. S20, Table S6), while the acid amount showed a sharp decrease after adding 0.2 wt% Ru (19.0 μmol/g), which may due to the severe coverage of acid sites on support by the ultra-highly dispersed Ru species. When the Ru content was increased to 0.5 wt%, the acid of Ru species played a positive role and enhancing the Lewis acid amount of 0.5Ru@NC-Al$_2$O$_3$. While further increasing the Ru loading, the Lewis acid amount exhibited a decreasing trend, because the increased acid sites introduced from the Ru species cannot compensate the loss of the acid sites caused by the covering of Ru on the surface of the Al$_2$O$_3$

support. The total amount of acidic sites decreased in the order of 0.5Ru@NC-Al$_2$O$_3$ > 1.0 Ru@NC-Al$_2$O$_3$ > 2.0Ru@NC-Al$_2$O$_3$ > 0.2Ru@NC-Al$_2$O$_3$ (Table S6), which was consistent with the NH$_3$-TPD analysis. This result was in good line with the yield of primary amine **2a** produced from furfural via reductive amination over xRu@NC-Al$_2$O$_3$ catalysts (Table 1). It was found that the B acid sites was inactive for the reductive amination of carbonyl compounds [37,42], which meant that this reaction was proceed at the L acid sites. The L acid sites on surface was reasonable for the conversion of imines intermediate toward desired primary amines.

X-ray photoelectron spectroscopy (XPS) was used to analyze the surface compositions and chemical valence state of xRu@NC-Al$_2$O$_3$. The XPS spectrums demonstrated the constitutions of C, O, N, Al, and Ru elements that implying the successfully loading of Ru species in xRu@NC-Al$_2$O$_3$ (Fig. S21). In the high-resolution Ru 3p spectra (Fig. 2D), the binding energies located around 462.5 eV (Ru 3p$_{3/2}$) and 484.9 eV (Ru 3p$_{1/2}$) were visible in xRu@NC-Al$_2$O$_3$, assigning to the Ru^0, while the rest of the peaks were corresponding to the form of Ru^{n+} species [43,44], demonstrating Ru ions were partially reduced to metallic Ru during the pyrolysis process. In addition, the binding energy of Ru^0 3p$_{3/2}$ (462.5 eV) core level was lower than that of Ru nanoparticles due to the strong interaction between Ru clusters and NC@ -Al$_2$O$_3$ support. For the C1s spectra partially overlapped by those of Ru 3d curves (Fig. 2E), the derived peaks centered at 284.8, 286.9, and 289.7 eV were attributed to C-C, C-N, and C═O bond, respectively. Two characteristic peaks at 281.3 eV (3d$_{5/2}$) and 284.5 eV (3d$_{3/2}$) were assigning to the Ru^0 clusters [45,46]. Meanwhile, the other two derived peaks appeared at 282.5 and 285.9 eV, which were consistent with Ru^{n+} 3d$_{3/2}$ and Ru^{n+} 3d$_{1/2}$ species [45,46], respectively. Obviously, When the loading of Ru was raised, the ratio of Ru^0/Ru^{n+} increased, as confirmed in both Fig. 2D and E. It is widely acknowledged that the metallic Ru species were beneficial to the hydrogenation steps. Nevertheless, excessive Ru^0 sites in catalyst would decrease the selectivity of desired primary amines [5,24], so that a superior yield of primary amines could be achieved over 0.5Ru@NC-Al$_2$O$_3$ in our catalytic system. The above results suggested that the catalytic performance of xRu@NC-Al$_2$O$_3$ was significantly influenced by the ratio of Ru^0 to Ru^{n+} species, and a suitable amount of Ru^0 could facilitate the activation of H$_2$ and the desorption of imines and Schiff bases intermediates. As for the valence of N center, three typical binding energies located around 398.6, 399.9, and 401.2 eV were observed (Fig. 2F), ascribing to the pyridinic N, pyrrolic N, and graphitic N [47,48], respectively. Remarkably, a peak at 399.2 eV attributing to the Ru-N bond was visible [47,48], further demonstrating the presence of Ru-N interaction in xRu@NC-Al$_2$O$_3$ complexes. The coordination of Ru to N species would help to stabilize the Ru sites and prevent its sintering and leaching.

These results above suggested that the combination of metal-acid dual active sites contributed to the excellent catalytic performance of reductive amination over 0.5Ru@NC-Al$_2$O$_3$ catalysts. The metallic Ru was beneficial to the activation of H$_2$ molecular in the hydrogenation step, while the L acid sites was responsible for the activation of C═N bonds in the in situ formed imines and Schiff base and their subsequent transformation to the desired primary amines [5,38]. Thus, the 0.5Ru@NC-Al$_2$O$_3$ catalysts with suitable Ru^0 percentage and highest total number of acidic sites cooperated well to promote the reductive amination and exhibited the highest yield of primary amine.

3.4. Optimization and stability of 0.5Ru@NC-Al$_2$O$_3$ catalyst

Besides the intrinsic structure of Ru@NC-Al$_2$O$_3$ catalyst, the effect of reaction conditions on catalytic performance were also systematically investigated. The temperature had a significant effect on the reductive amination of **1a**. Only 12.1% yield of **2a** was obtained at 60 ℃ with some **2b** and **2d** byproducts, whereas it boosted up to 96.6% at 100 ℃, and then displayed a decreasing trend with the increase of temperature (Table S7). Additionally, the effect of pressure exhibited a similar
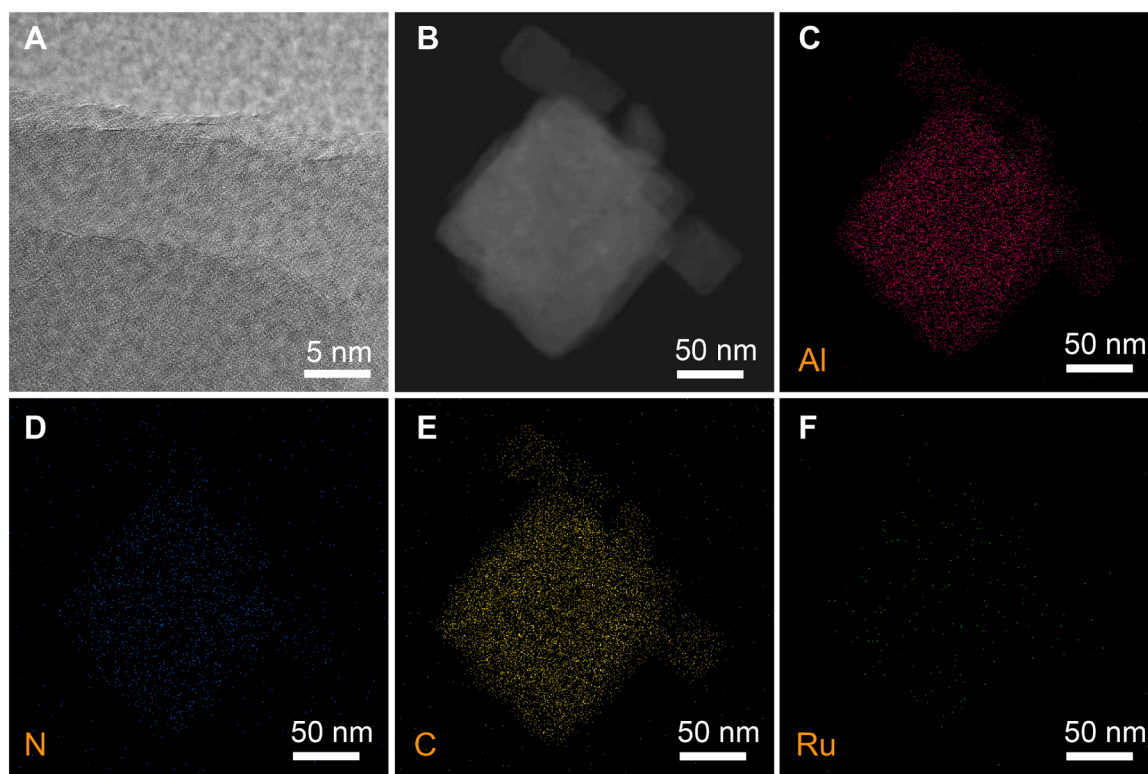
Fig. 3. . (A,B) HR-TEM images, and corresponding EDS element mappings of (C) Al, (D) N, (E) C, and (F) Ru species of 0.5Ru@NC-Al$_2$O$_3$ catalyst after recycling test.
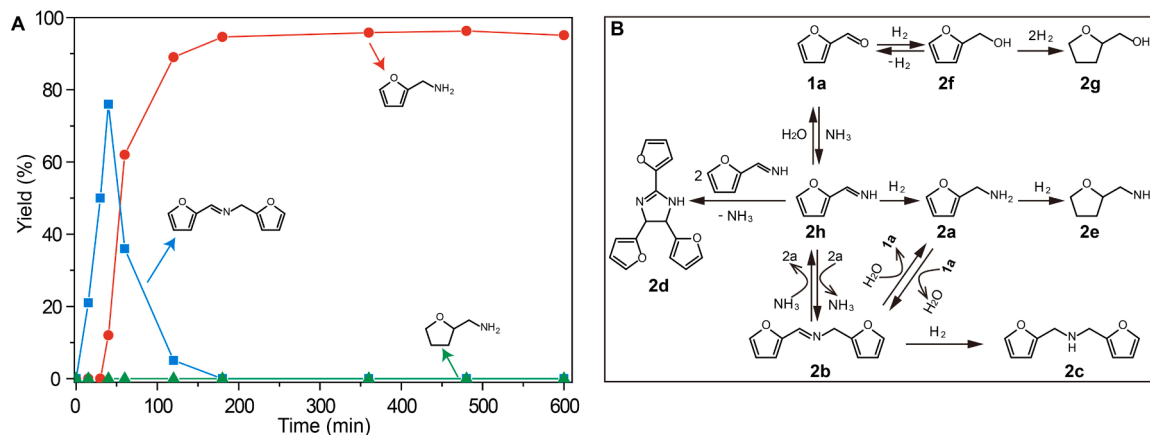

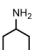**Fig. 4.** (A) Time course of the reductive amination of furfural over 0.5Ru@NC-Al$_2$O$_3$ catalyst. Reaction conditions: furfural (1 mmol), catalyst (50 mg), NH$_3$ (7 M in MeOH, 6 mL), temperature (100 °C), H$_2$ pressure (2.0 MPa), stirring speed (600 rpm). (B) The plausible reaction pathway for the reductive amination of furfural over 0.5Ru@NC-Al$_2$O$_3$ catalyst.
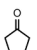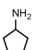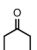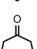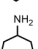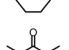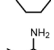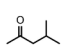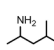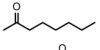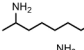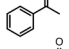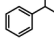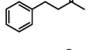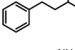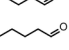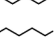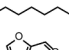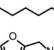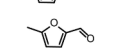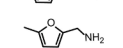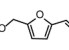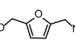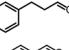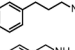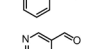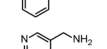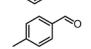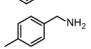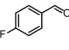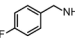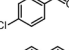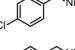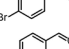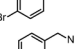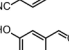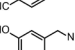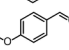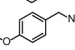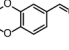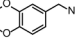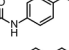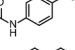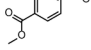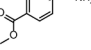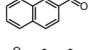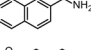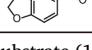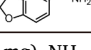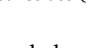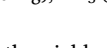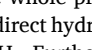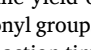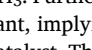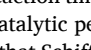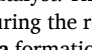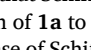
tendency to that of temperature, and an excellent 96.6% yield of **2a** was achieved under the optimized reaction conditions of 100 °C and 2 MPa H$_2$ (Table S8). The 0.5Ru@NC-Al$_2$O$_3$ catalyst could be recycled for at least five consecutive runs without obvious decay in activity and desired product selectivity at different **2a** yield level (~60% and ~95%, Fig. S22), suggesting the excellent retrievability and reusability. We noted that no detectable Ru reflection signal was observed for the spent 0.5Ru@NC-Al$_2$O$_3$ catalyst (Fig. S23), implying the robust stability and uniformly dispersion of Ru species. Further, the recovered 0.5Ru@NC-Al$_2$O$_3$ catalyst showed similar morphology to the pristine one, and EDS mapping of Ru matched well with Al, N, and C element across the single particle (Fig. 3). Besides, the concentrations of Ru species in reaction solution were below the detectable limit of ICP-OES, confirmed the negligible leaching of Ru species. The XPS of Ru 3p displayed similar

percentage of Ru^0 in spent catalyst in comparison to the fresh one, further indicating the stability of 0.5Ru@NC-Al$_2$O$_3$ catalyst (Fig. S24). All these results demonstrated the excellent stability of 0.5Ru@NC-Al$_2$O$_3$ catalyst.

3.5. Mechanism discussion

In order to investigate the reaction mechanism of reductive amination, the products distribution depended on time was performed. As shown in Fig. 4A, **1a** was completely converted within 15 min, and large amount of Schiff base (**2b**, secondary imine) was formed and reached the maximum yield of 76% at 40 min. At the same time, **2a** was produced and the yield increased gradually with the decrease of **2b**, while the hydrogenated products like furfural alcohol (**2 f**), **2e**, and **2 g** were not

Table 2
Conversion of various aldehydes and ketones to primary amines over 0.5Ru@NC-Al$_2$O$_3$ catalyst.

Entry	Substrate	Product	Time (h)	Yield (%)
1			3	99
2			5	95
3			5	96
4			3	98
5			5	94
6			5	91
7			5	92
8			5	93
9			3	99
10			3	95
11			5	91
12			3	95
13			6	90
14			4	97
15			8	92
16			5	96
17			5	96
18			5	97
19			5	93
20			5	91
21			5	90
22			5	94
23			5	93
24			5	91
25			6	91
26			6	89
27			6	92
28			8	88
29			8	90

Reaction conditions: substrate (1 mmol), catalyst (50 mg), NH$_3$ (7 M in MeOH, 6 mL), temperature (100 °C), H$_2$ pressure (2.0 MPa), stirring speed (600 rpm).

detected during the whole process, even after the yield of **2a** reached 96%, revealing the direct hydrogenation of carbonyl groups was difficult in the presence of NH$_3$. Further prolonging the reaction time to 10 h, the **2a** yield kept constant, implying the excellent catalytic performance of 0.5Ru@NC-Al$_2$O$_3$ catalyst. This result indicated that Schiff base was the key intermediate during the reductive amination of **1a** to **2a** due to the direct evidence of **2a** formation was at the expense of Schiff base, which was in line with precious reported literatures [10,23,24]. In addition, we speculated that the conversion of Schiff base to primary amines was the

rate-determining step because of its rapid formation while slowly consumption. Based on the above discussion, a possible mechanism was proposed for the reductive amination of carbonyl compounds to primary amines using NH$_3$ as the nitrogen source and H$_2$ as the hydrogen source (Fig. 4B). Initially, the intermediate imine (**2 h**, unstable and cannot be detected by existing equipment) was rapidly formed from the condensation of **1a** and NH$_3$, and subsequently reacted with **2a** to produce the stable intermediate of Schiff base (secondary imine, **2b**) quickly. Then the generated Schiff base was further transferred to targeted primary

amine relatively slowly by hydrogenolysis.

3.6. Scope of the substrates

Encouraged by the outstanding catalytic performance of 0.5Ru@NC-Al$_2$O$_3$ catalyst, it was employed to the reductive amination of a wide range of substrates including aldehydes and ketones under the optimized conditions, and good to excellent yield of corresponding primary amines were achieved (Table 2). Cyclic ketones with different carbon numbers (Table 2, entries 1–3), linear aliphatic ketones (Table 2, entries 4–6), and aromatic ketones (Table 2, entries 7,8) could smoothly converted to the desired primary amines with high yield (91–99%). Compared with ketones, the efficient reductive amination of aldehydes to primary amines with high selectivity was more challenging due to their higher reactivity. Aliphatic aldehydes with different carbon numbers were good substrates and displayed high yield of corresponding primary amines (Table 2, entries 9–11). In addition, the biomass-derived platform chemicals like furfural, 5-methyfurfural, and 5-hydroxymethylfurfural could also be transformed to primary amines with high yield (90–97%, Table 2, entries 12–14). Aromatic aldehydes (Table 2, entries 15–17), in particular for the heterocyclic aldehydes such as 3-pyridinecarboxaldehyde which was poison to the noble metal catalyst, the reductive amination could be performed effectively. More importantly, the aryl aldehydes with sensitive functional groups, including methyl (Table 2, entry 18), halogens (Table 2, entries 19–21), nitril (Table 2, entry 22), phenolic hydroxyl (Table 2, entry 23), methoxy (Table 2, entries 24 and 25), acetamido (Table 2, entry 26), esters (Table 2, entry 27), and more challenging groups (Table 2, entries 28 and 29), could all be converted to their corresponding primary amines with high yields, while those sensitive functional groups remained unchanged. These results demonstrated that the 0.5Ru@NC-Al$_2$O$_3$ catalyst possessed high activity and selectivity, as well as outstanding tolerance to a broad range of substrates, which is a promising candidate for practical applications.

4. Conclusion

In summary, we developed a facile and versatile approach for the in-situ formation of ultrasmall Ru clusters encapsulated in nitrogen-dopped porous carbon supported on alumina matrix from MOF chelated atomically dispersed Ru species. The resulting 0.5Ru@NC-Al$_2$O$_3$ catalyst exhibited high activity and selectivity for the primary amines via reductive amination of a broad variety of carbonyl compounds including heterocyclic, aliphatic, aryl ketones or aldehydes with sensitive functional groups. Besides, it displayed excellent robust stability which enabled to be recycled for at least five consecutive times without a loss of activity and selectivity. The combination of ultrasmall Ru clusters stabilized by N-doped porous carbon and high Lewis acidic sites might be the key to the observed high activity/selectivity, and long-term stability. We believe that this work provided new insight to the efficient and durable catalysts for heterogeneous catalysis especially in the pharmaceutical field.

CRediT authorship contribution statement

Yushan Wu: Investigation, Data curation, Formal analysis, Writing – original draft. **Di Xu:** Resources. **Yanfei Xu**: Investigation. **Xin Tian**: Formal analysis. **Mingyue Ding**: Supervision, Writing – review & editing, Funding acquisition.

Declaration of Competing Interest

The authors declare that they have no known competing financial interests or personal relationships that could have appeared to influence the work reported in this paper.

Data availability

Data will be made available on request.

Appendix A. Supporting information

Supplementary data associated with this article can be found in the online version at doi:10.1016/j.apcatb.2023.123462.

References

[1] O.I. Afanasyev, E. Kuchuk, D.L. Usanov, D. Chusov, Reductive amination in the synthesis of pharmaceuticals, Chem. Rev. 119 (2019) 11857–11911.

[2] T. Irrgang, R. Kempe, Transition-metal-catalyzed reductive amination employing hydrogen, Chem. Rev. 120 (2020) 9583–9967.

[3] K. Murugesan, T. Senthamarai, V.G. Chandrashekhar, K. Natte, P.C.J. Kamer, M. Beller, R.V. Jagadeesh, Catalytic reductive aminations using molecular hydrogen for synthesis of different kinds of amines, Chem. Soc. Rev. 49 (2020) 6273–6328.

[4] N.U.D. Reshi, V.B. Saptal, M. Beller, J.K. Bera, Recent progress in transition-metal-catalyzed asymmetric reductive amination, ACS Catal. 11 (2021) 13809–13837.

[5] C. Xie, J. Song, M. Hua, Y. Hu, X. Huang, H. Wu, G. Yang, B. Han, Ambient-temperature synthesis of primary amines via reductive amination of carbonyl compounds, ACS Catal. 10 (2020) 7763–7772.

[6] M. Sheng, S. Fujita, S. Yamaguchi, J. Yamasaki, K. Nakajima, S. Yamazoe, T. Mizugaki, T. Mitsudome, Single-crystal cobalt phosphide nanorods as a high-performance catalyst for reductive amination of carbonyl compounds, JACS Au 1 (2021) 501–507.

[7] H. Zou, J. Chen, Efficient and selective approach to biomass-based amine by reductive amination of furfural using Ru catalyst, Appl. Catal. B Environ. 309 (2022), 121262.

[8] R.V. Jagadeesh, K. Murugesan, A.S. Alshammari, H. Neumann, M.M. Pohl, J. Radnik, M. Beller, MOF-derived cobalt nanoparticles catalyze a general synthesis of amines, Science 358 (2017) 326–332.

[9] T. Senthamarai, K. Murugesan, J. Schneidewind, N.V. Kalevaru1, W. Baumann, H. Neumann, P.C.J. Kamer, M. Beller, R.V. Jagadeesh, Simple ruthenium-catalyzed reductive amination enables the synthesis of a broad range of primary amines, Nat. Commun. 9 (2018) 4123.

[10] H. Qi, J. Yang, F. Liu, L. Zhang, J. Yang, X. Liu, L. Li, Y. Su, Y. Liu, R. Hao, A. Wang, T. Zhang, Highly selective and robust single-atom catalyst Ru$_1$/NC for reductive amination of aldehydes/ketones, Nat. Commun. 12 (2021) 3295.

[11] Y. Wang, S. Furukawa, X. Fu, N. Yan, Organonitrogen chemicals from oxygen-containing feedstock over heterogeneous catalysts, ACS Catal. 10 (2019) 311–335.

[12] T. Wang, J. Ibañez, K. Wang, L. Fang, M. Sabbe, C. Michel, S. Paul, M. Pera-Titus, P. Sautet, Rational design of selective metal catalysts for alcohol amination with ammonia, Nat. Catal. 2 (2019) 773–779.

[13] H. Guo, B. Wang, P. Qiu, R. Gao, M. Sun, L. Chen, N,S-codoped carbon shells embedded with ultrafine Co NPs for reductive amination with formic Acid, ACS Sustain. Chem. Eng. 7 (2019) 8876–8884.

[14] K. Murugesan, M. Beller, R.V. Jagadeesh, Reusable nickel nanoparticles-catalyzed reductive amination for selective synthesis of primary amines, Angew. Chem. Int. Ed. 58 (2019) 5064–5068.

[15] Z. Yuan, B. Liu, P. Zhou, Z. Zhang, Q. Chi, Preparation of nitrogen-doped carbon supported cobalt catalysts and its application in the reductive amination, J. Catal. 370 (2019) 347–356.

[16] T. Senthamarai, V.G. Chandrashekhar, M.B. Gawande, N.V. Kalevaru, R. Zboril, P. C.J. Kamer, R.V. Jagadeesh, M. Beller, Ultra-small cobalt nanoparticles from molecularly defined Co–salen complexes for catalytic synthesis of amines, Chem. Sci. 11 (2020) 2973–2981.

[17] K. Zhou, H. Liu, H. Shu, S. Xiao, D. Guo, Y. Liu, Z. Wei, X. Li, A comprehensive study on the reductive amination of 5-hydroxymethylfurfural into 2,5-bisamino-methylfuran over Raney Ni through DFT calculations, ChemCatChem 11 (2019) 2649–2656.

[18] B. Zheng, J. Xu, J. Song, H. Wu, X. Mei, K. Zhang, W. Han, W. Wu, M. He, B. Han, Nanoparticles and single atoms of cobalt synergistically enabled low-temperature reductive amination of carbonyl compounds, Chem. Sci. 13 (2022) 9047–9055.

[19] C. Dong, Y. Wu, H. Wang, J. Peng, Y. Li, C. Samart, M. Ding, Facile and efficient synthesis of primary amines via reductive amination over a Ni/Al₂O₃ catalyst, ACS Sustain. Chem. Eng. 9 (2021) 7318–7327.

[20] X. Zhuang, J. Liu, S. Zhong, L. Ma, Selective catalysis for the reductive amination of furfural toward furfurylamine by graphene-co-shelled cobalt nanoparticles, Green. Chem. 24 (2022) 271–284.

[21] G. Hahn, P. Kunnas, N. de Jonge, R. Kempe, General synthesis of primary amines via reductive amination employing a reusable nickel catalyst, Nat. Catal. 2 (2019) 71–77.

[22] C. Bäumler, C. Bauer, R. Kempe, The synthesis of primary amines through reductive amination employing an Iron catalyst, ChemSusChem 13 (2020) 3110–3114.

[23] S. Song, Y. Wang, N. Yan, A remarkable solvent effect on reductive amination of ketones, Mol. Catal. 454 (2018) 87–93.

[24] T. Komanoya, T. Kinemura, Y. Kita, K. Kamata, M. Hara, Electronic effect of ruthenium nanoparticles on efficient reductive amination of carbonyl compounds, J. Am. Chem. Soc. 139 (2017) 11493–11499.

[25] D. Chandra, Y. Inoue, M. Sasase, M. Kitano, A. Bhaumik, K. Kamata, H. Hosono, M. Hara, A high performance catalyst of shape-specific ruthenium nanoparticles for production of primary amines by reductive amination of carbonyl compounds, Chem. Sci. 9 (2018) 5949–5956.

[26] D. Deng, Y. Kita, K. Kamata, M. Hara, Low-temperature reductive amination of carbonyl compounds over Ru deposited on Nb₂O₅·nH₂O, ACS Sustain. Chem. Eng. 7 (2019) 4692–4698.

[27] W. Guo, T. Tong, X. Liu, Y. Guo, Y. Wang, Morphology-tuned activity of Ru/Nb₂O₅ catalysts for ketone reductive amination, ChemCatChem 11 (2019) 4130–4138.

[28] C. Dong, H. Wang, H. Du, J. Peng, Y. Cai, S. Guo, J. Zhang, C. Samart, M. Ding, Ru/ HZSM-5 as an efficient and recyclable catalyst for reductive amination of furfural to furfurylamine, Mol. Catal. 482 (2020), 110755.

[29] F. Fathieh, M.J. Kalmutzki, E.A. Kapustin, P.J. Waller, J. Yang, O.M. Yaghi, Practical water production from desert air, Sci. Adv. 4 (2018) eaat3198.

[30] W. Xu, O.M. Yaghi, Metal-organic frameworks for water harvesting from air, anywhere, anytime, ACS Cent. Sci. 6 (2020) 1348–1354.

[31] N. Hanikel, X. Pei, S. Chheda, H. Lyu, W. Jeong, J. Sauer, L. Gagliardi, O.M. Yaghi, Evolution of water structures in metal-organic frameworks for improved atmospheric water harvesting, Science 374 (2021) 454–459.

[32] Y. Qian, S. Jiang, Y. Li, Z. Yi, J. Zhou, J. Tian, Ning Lin, Y. Qian, Water-induced growth of a highly oriented mesoporous graphitic carbon nano spring for fast potassium-ion adsorption/intercalation storage, Angew. Chem. Int. Ed. 58 (2019) 18108–18115.

[33] M. Fan, Q. Yuan, Y. Zhao, Z. Wang, A. Wang, Y. Liu, K. Sun, J. Wu, L. Wang, J. Jiang, A facile "double-catalysts" approach to directionally fabricate pyridinic N-B-pair-doped crystal graphene nanoribbons/amorphous carbon hybrid electrocatalysts for efficient oxygen reduction reaction, Adv. Mater. 34 (2022) 2107040.

[34] Y. Wang, G. Wang, L.I. van der Wal, K. Cheng, Q. Zhang, K.P. de Jong, Y. Wang, Visualizing element migration over bifunctional metal-zeolite catalysts and its impact on catalysis, Angew. Chem. Int. Ed. 60 (2021) 17735–17743.

[35] Y. Shi, Z. Li, J. Wang, R. Zhou, Synergistic effect of Pt/Ce and USY zeolite in Pt-based catalysts with high activity for VOCs degradation, Appl. Catal. B Environ. 286 (2021), 119936.

[36] K. Sasaki, J.A.H. Gaitan, T. Okue, S. Matoba, Y. Tokuda, K. Miyake, Y. Uchida, N. Nishiyama, Amorphous alumino silicate nanosheets as universal precursors for the synthesis of diverse zeolite nanosheets for polymer-cracking reactions, Angew. Chem. Int. Ed. 61 (2022), e202213773.

[37] J.H. Cho, S.H. An, T.-S. Chang, C.-H. Shin, Effect of an alumina phase on the reductive amination of 2-propanol to monoisopropylamine over Ni/Al₂O₃, Catal. Lett. 146 (2016) 811–819.

[38] Z. Yu, W. Jin, Q. Jiang, Brønsted acid activation strategy in transition-metal catalyzed asymmetric hydrogenation of N-unprotected imines, enamines, and N-heteroaromatic compounds, Angew. Chem. Int. Ed. 51 (2012) 6060–6072.

[39] S. Hu, J. Liu, G. Ye, X. Zhou, M.-O. Coppens, W. Yuan, Effect of external surface diffusion barriers on platinum/beta-catalyzed isomerization of n-pentane, Angew. Chem. Int. Ed. 60 (2021), 14394-143.

[40] Z. Chen, Y. Ye, X. Feng, Y. Wang, X. Han, Y. Zhu, S. Wu, S. Wang, W. Yang, L. Wang, J. Zhang, High-density frustrated Lewis pairs based on Lamellar Nb₂O₅ for photocatalytic non-oxidative methane coupling, Nat. Commun. 14 (2023) 2000.

[41] Y.T. Kima, K.-D. Junga, E.D. Park, Gas-phase dehydration of glycerol over silica–alumina catalysts, Appl. Catal. B Environ. 107 (2011) 177–187.

[42] S.R. Kirumakki, M. Papadaki, K.V.R. Chary, N. Nagaraju, Reductive amination of cyclohexanone in the presence of cyclohexanol over zeolites H and HY, J. Mol. Catal. A Chem. 321 (2010) 15–21.

[43] J. Wang, Z. Wei, S. Mao, H. Li, Y. Wang, Highly uniform Ru nanoparticles over N-doped carbon: pH and temperature-universal hydrogen release from water reduction, Energy Environ. Sci. 11 (2018) 800–806.

[44] P. Su, W. Pei, X. Wang, Y. Ma, Q. Jiang, J. Liang, S. Zhou, J. Zhao, J. Liu, G.Q. (Max) Lu, Exceptional electrochemical HER performance with enhanced electron transfer between Ru nanoparticles and single atoms dispersed on a carbon substrate, Angew. Chem. Int. Ed. 60 (2021) 16044–16050.

[45] Y.-T. Lia, S.-H. Zhang, G.-P. Zheng, P. Liu, Z.-K. Peng, X.-C. Zheng, Ultrafine Ru nanoparticles anchored to porous g-C₃N₄ as efficient catalysts for ammonia borane hydrolysis, Appl. Catal. A Gen. 595 (2020), 117511.

[46] Y. Guo, S. Mei, K. Yuan, D.-J. Wang, H.-C. Liu, C.-H. Yan, Y.-W. Zhang, Low-temperature CO₂ methanation over CeO₂-supported Ru single atoms, nanoclusters, and nanoparticles competitively tuned by strong metal-support interactions and H-spillover effect, ACS Catal. 8 (2018) 6203–6215.

[47] T. Li, H. Lin, X. Ouyang, X. Qiu, Z. Wan, In situ preparation of Ru@N-doped carbon catalyst for the hydrogenolysis of lignin to produce aromatic monomers, ACS Catal. 9 (2019) 5828–5836.

[48] H. Yao, X. Wang, K. Li, C. Li, C. Zhang, J. Zhou, Z. Cao, H. Wang, M. Gu, M. Huang, H. Jiang, Strong electronic coupling between ruthenium single atoms and ultrafine nanoclusters enables economical and effective hydrogen production, Appl. Catal. B Environ. 312 (2022), 121378.